The "Meteorite meter": A handheld instrument for the combined measurement of magnetic susceptibility and electrical conductivity, with application to meteorite identification and classification

Minoru Uehara, Jérôme Gattacceca

The Meteoritical Society

Meteoritics & Planetary Science 1–13 (2023)
doi: 10.1111/maps.14087

The "Meteorite meter": A handheld instrument for the combined measurement of magnetic susceptibility and electrical conductivity, with application to meteorite identification and classification

Minoru UEHARA and Jérôme GATTACCECA*

CNRS, IRD, INRAE, CEREGE, Aix Marseille Univ, Aix-en-Provence, France
***Correspondence**
Jérôme Gattacceca, CNRS, IRD, INRAE, CEREGE, Aix Marseille Univ, Aix-en-Provence, France.
Email: gattacceca@cerege.fr

(Received 03 April 2023; revision accepted 20 September 2023)

Abstract–We developed a simple, handheld, and user-friendly magnetic susceptibility meter specialized for the identification of meteorites. The measurement is based on an LC resonance circuit. When provided with a rough estimate of the sample mass, the instrument displays directly the mass-normalized magnetic susceptibility expressed in $\log\chi_m$ (with χ_m in 10^{-9} m^3 kg^{-1}), a parameter that is widely used in the classification of meteorites. Moreover, the measurement of the impedance of the LC resonator provides a proxy of the electrical conductivity (*C*-index) that can be helpful to distinguish metal-bearing samples from magnetite-bearing samples. This *C*-index offers an additional diagnostic for the identification of meteorites. Our tests demonstrate that the precision and the accuracy of this instrument called "Meteorite meter" (MetMet) are sufficient to allow distinguishing most meteorites from most terrestrial rocks, for a minimum recommended sample mass of 5 g. The distinction of some meteorite groups is also possible, in particular the separation of the three ordinary chondrite groups. Meteorite hunters, collectors, and curators and non-specialists, including children, can use this instrument as a guidance in the identification and classification of meteorites. This kind of instrument has an immense advantage over the widely used testing of meteorites with magnets, as it does not affect the paleomagnetic records of meteorites that are highly valuable for scientists.

INTRODUCTION

Over 70,000 meteorites have been registered by the Meteoritical Society to date, and this number has increased by more than 2000 per year since 2014 (see the Meteoritical Bulletin Database, https://www.lpi.usra.edu/meteor/). The classification of so many meteorites is a significant burden for the meteorite scientist community, all the more because 90% of the non-Antarctic meteorites (1250 meteorites for the year 2020 for instance) are classified by only 10 scientists worldwide (Gattacceca et al., 2021). The majority of these meteorites are ordinary chondrites (84% in 2020). The classic tools for meteorite classification are petrography (optical microscopy and/or scanning electron microscopy) and electron probe microanalyses (EPMA). Petrographic observations are an unavoidable step for the classification of any meteorite. As far as ordinary chondrites are concerned, these observations are necessary to determine if a meteorite is indeed an ordinary chondrite, and to determine the petrographic type of the chondrite. They can also provide additional, but not strictly necessary classification parameters such as shock stage or terrestrial weathering grade.

Alternative methods have been developed to accelerate the classification of ordinary chondrites by avoiding the relatively costly and time-consuming EPMA. They rely on the determination of the silicate composition by other methods (oil immersion, energy-dispersive

spectrometry, x-ray diffraction), or on the estimate of bulk metal content (magnetic susceptibility). Indeed, ordinary chondrite main groups are readily separated by their olivine and low-Ca pyroxene composition when equilibrated (e.g., Keil & Frederiksson, 1964), or by their metal content, be they equilibrated or not (e.g., Jarosewich, 1990). Chondrule size can also be used to distinguish between unequilibrated H, L, or LL chondrites (e.g., Metzler, 2018).

Oil immersion, that has been widely used for the classification of equilibrated ordinary chondrites (EOC) collected in the framework of the ANSMET program (Lunning et al., 2012), is now being abandoned as it resulted in relatively frequent misclassification due to the uncertainty on the estimate of silicate composition. X-ray diffraction allows the classification of EOC, but remains relatively time-consuming and has significant uncertainty (Di Cecco et al., 2022). Handheld XRF has been shown to distinguish successfully the three ordinary chondrite groups based on their bulk Fe/Mn ratio and is another powerful tool to distinguish some achondrite groups (Zurfluh et al., 2011). The bulk metal content also allows separating ordinary chondrites into the H, L, and LL groups. It can be estimated by chemical analyses (e.g., Jarosewich, 1990), but this is a time-consuming and meteorite-consuming process. Magnetic susceptibility, on the other hand, has proved to be a fast and nondestructive way to estimate the bulk metal content and hence a useful tool to classify ordinary chondrites (e.g., Consolmagno et al., 2006; Rochette et al., 2003). Besides ordinary chondrite, magnetic susceptibility can also help for classification of non-ordinary chondrites (Rochette et al., 2008) and achondrites (Rochette et al., 2009). The magnetic measurements can be easily performed in the field, allowing for initial screening and pairing of meteorites (Folco et al., 2006). It is noteworthy that magnetic susceptibility measurements are highly preferable to the use of hand magnets. Indeed, they offer a much better diagnostic, and most of all, they do not affect the paleomagnetic record of meteorites that is of high scientific value (e.g., Weiss et al., 2010), but is erased completely and instantaneously when using strong magnets (Gattacceca & Rochette, 2004; Savitsky, 2023; Vervelidou et al., 2023).

In this report, we present a new small, portable, and easy-to-use instrument that can be used to assess quickly the magnetic susceptibility of meteorites. It can be used for screening meteorite-looking rocks (meteorwrongs) in the field, it can contribute to meteorite classification, and it is also particularly suited for outreach activities. In addition to magnetic susceptibility, it provides an estimate of the electrical conductivity that is a useful parameter to distinguish magnetite-rich from metal-rich rocks.

INTEREST OF A NEW MAGNETIC SUSCEPTIBILITY METER DEDICATED TO METEORITES

Problems of Units and Mass Normalization

We distinguish here laboratory magnetic susceptibility meters and "handheld" ones. The former are more expensive and not really portable. Moreover, their sensitivity is exceedingly good for the purpose of meteorite identification and classification because meteorites are usually very magnetic compared to terrestrial rocks, and their magnetic susceptibility range over three orders of magnitude. Few handheld instruments, such as the SM30 from ZH instruments, are available and have shown to be suited for meteorite classification (Folco et al., 2006), provided that a specific calibration is performed (Gattacceca et al., 2004).

All available magnetic susceptibility meters display the volume magnetic susceptibility in SI unit (χ_v), by normalizing the total susceptibility (m^3) by an a priori nominal volume. However, for the purpose of classification, the mass normalized magnetic susceptibility is used, because it is simpler and more accurate to measure the mass of a sample rather than its volume. Most works about the magnetic susceptibility of meteorites report it in units of $\log\chi_m$, where χ_m is the mass-normalized magnetic susceptibility (also called specific magnetic susceptibility) and is expressed in 10^{-9} m^3 kg^{-1} to end up on a $\log\chi_m$ scale conveniently ranging from 2 to 6 for meteorites.

When using an instrument providing volume susceptibility, the mass-normalized value $\log\chi_m$ is obtained by

$$\log_{10}\left(\frac{\chi_v}{\rho}\times 10^9\right), \quad (1)$$

where ρ is the density of the sample in m^3 kg^{-1}. Although this calculation is trivial for scientists in the laboratory, it is rather complicated to perform mentally in the field, or to be done easily by people who are not familiar with basic mathematical concepts (logarithms, normalization) or people not familiar with the subtleties of magnetic units (this latter category encompassing most of meteorite scientists in fact).

An instrument providing directly the log χ_m value that can be readily compared to the published average values for meteorites is therefore desirable.

Overlapping Susceptibility Ranges and Terrestrial Weathering

Although the ordinary chondrite groups are well separated by their magnetic susceptibility, when considering all meteorites (non-ordinary chondrites, achondrites), there

is significant overlap of magnetic susceptibility values between meteorite groups (see fig. 3 in Rochette et al., 2012). Moreover, terrestrial weathering of meteorites leads to the transformation of FeNi metallic minerals into iron oxides and iron oxyhydroxides (e.g., Munayco et al., 2013; Uehara et al., 2012). Because iron oxyhydroxides and all iron oxides except magnetite and maghemite have a lower magnetic susceptibility than metallic FeNi minerals, terrestrial weathering result in a decrease of magnetic susceptibility, which can lead to and overlap between, for example, the different groups of ordinary chondrites (see fig. 4 in Rochette et al., 2012). For weathered ordinary chondrites, the magnetic susceptibility must therefore be interpreted with regard to their weathering grade as defined by Wlotzka (1993), even though there remains some unresolvable overlap from weathering grade W3 and up.

Because iron oxides and oxyhydroxides are less conductive than FeNi metal, an estimate of the electrical conductivity of the rocks can help separate iron oxide-rich and metal-rich rocks. This would help resolving some of the inter-group overlapping of magnetic susceptibility, identifying magnetic metal-free meteorwrongs, and would offer the possibility of estimating the bulk weathering grade of metal-bearing meteorites.

An instrument providing, at the same time as magnetic susceptibility, an estimate of electrical conductivity of rocks is therefore desirable.

Proposed Solution

Based on the limitations raised in the two preceding parts, we have developed a handheld magnetic susceptibility meter whose output are the mass normalized magnetic susceptibility in units of log χ_m, and an estimate of the electrical conductivity. This new instrument has been so far used successfully for outreach activities, during meteorite collecting campaigns in hot deserts (Atacama, Sahara) and Antarctica, and in the laboratory for meteorite classification. In this paper, we describe the basic theory of operation and the result of the measurements of a collection of meteorites and terrestrial rocks and minerals. We also discuss the potential of this instrument to identify meteorites and to assist in their classification. This instrument was developed in the framework of the outreach project "VigieCiel" (www.vigie-ciel.org), the citizen science counterpart of the FRIPON meteor detection network (Colas et al., 2020).

METHODS

Description and Calibration of the Instrument

The developed magnetic susceptibility meter (called "Meteorite meter," and abbreviated as MetMet) consists of a custom-made coil, circuit board with a simple LCD indicator, and a rotative switch (Figure 1a). A Li battery (CR2032) powers the circuit and can sustain relatively long operations (e.g., several weeks of meteorite hunting mission, several months of workshop, several years for occasional use in the laboratory). The coil and a capacitor on the circuit board consist a simple LC oscillator with a positive feedback generated by an amplifier U and a feedback resistance R (Figure 1b), where L and C stands for inductance (coil, in H) and the capacitance (capacitor, in F). When there is no rock sample in the vicinity of the coil (state i of Figure 1b), the frequency of this oscillator f (Hz) is given by

$$f_{\text{air}} = \frac{2\pi}{\sqrt{LC}}. \tag{2a}$$

Since the capacitance is constant, the variation of f reflects the difference of the variable L. When a rock sample with a non-null susceptibility approaches the coil, the inductance increases (state ii of Figure 1b). The resulting frequency is

$$f_{\text{sample}} = \frac{2\pi}{\sqrt{(L+\Delta)C}}, \tag{2b}$$

where Δ is the increased inductance due to the sample's susceptibility. The ratio of these two frequencies gives us the magnetic susceptibility of the sample as Δ to the intrinsic inductance of the coil L,

$$K = \left(\frac{f_{\text{air}}}{f_{\text{sample}}}\right)^2 - 1 = \frac{\Delta}{L}. \tag{3}$$

This K value is dimensionless and proportional to the volume magnetic susceptibility of the sample χ_v in SI unit, assuming that the pick-up coil and the circuit are stable during two measurements. The actual susceptibility can be calculated after calibrations. The nominal magnetic field applied by the MetMet is 100 kHz in frequency and 2.5 A m^{-1} in amplitude.

There are two calibration factors for this instrument. The first is a factor of sensitivity α (in m^3 kg^{-1}), and the second is a dimensionless factor related to the size of the sample β that is a function of the mass m. Using these two factors, the instrument estimates the mass-normalized magnetic susceptibility as

$$\chi_m(m) = \frac{\alpha K}{\beta(m)}. \tag{4}$$

The sensitivity factor α was determined by measuring flat concrete blocks that were large enough to be

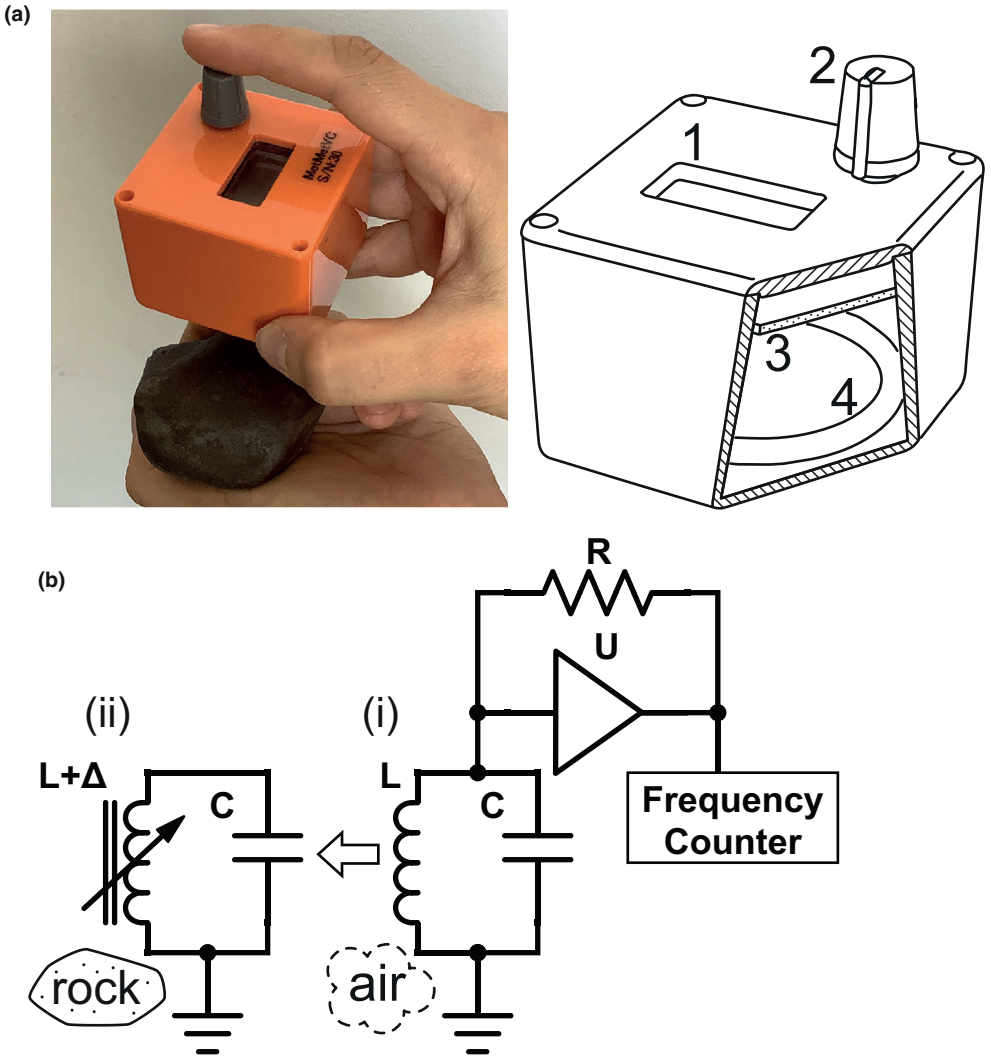

FIGURE 1. (a) Operation of the Meteorite meter (left), and sketch of the instrument (right). 1. LCD indicator, 2. knob connected to a rotary encoder with push switch, 3. printed circuit board, 4. pick-up coil connected to the circuit board. (b) Simplified circuit diagram of the measurement. The pick-up coil L and the capacitor C form a resonator driven by the amplifier U and the feedback resistance R, building a simple LC oscillator. The frequency counter measures the frequency of the oscillation.

considered as semi-infinite (the raw data are available in Table S2). The susceptibility of these blocks was also measured using a KLY-2 magnetic susceptibility meter from Agico operating at 920 Hz. This provided a value $\alpha = 3.58 \times 10^{-3}$ m^3 kg^{-1} (Figure 2a). Smaller samples provide smaller apparent magnetic susceptibilities, because a larger fraction of the sensitive zone of the coil is occupied by air (Figure 2b). Thus, the measurement must be calibrated depending on the size of the sample (see a detailed discussion on this topic in Gattacceca et al., 2004). To take this effect into account, we measured the same ellipsoidal basalt pebbles, used in Gattacceca et al. (2004) for the same purpose. These pebbles were collected on the Durance river banks close to Saint-Paul-lez-Durance (France) and have had their magnetic susceptibility measured with a KLY-2 instrument (Gattacceca et al., 2004). The raw calibration data are available in Table S3. Note that although the MetMet operates at 100 kHz and with a field amplitude of 2.5 A m^{-1}, which is different from the KLY-2 field conditions (920 Hz and 400 A m^{-1}), any field or frequency dependence of the magnetic susceptibility of the calibration basalt pebbles is taken into account by the calibration process. Moreover, using a SM150 instrument, we checked that the basalt calibration samples have negligible frequency dependence (only 1.2% between 63 Hz ad 16 kHz), which is confirmed by the identical values of magnetic susceptibility of these pebbles provided by the KLY2, operating at 920 Hz, and the SM30, operating at 8 kHz (Figure S1b).

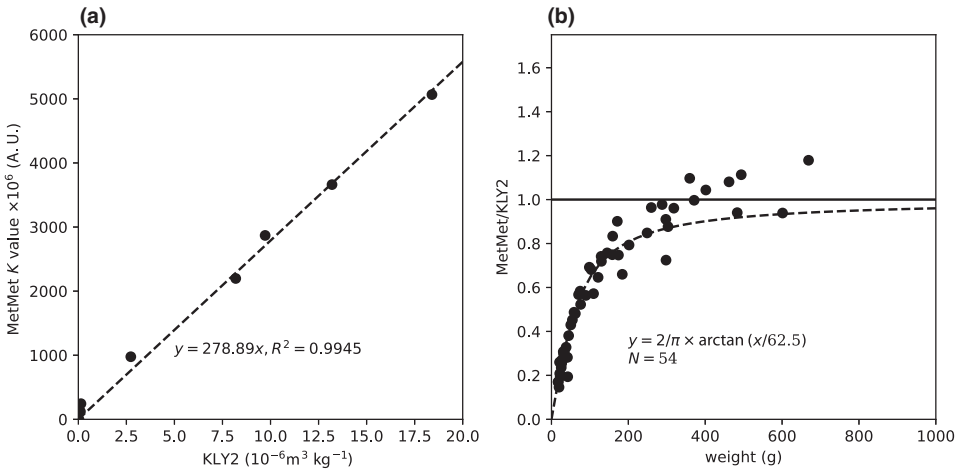

FIGURE 2. (a) Calibration of the sensitivity factor α. The x-axis shows the susceptibility measured using a KLY2 laboratory instrument, and the y-axis shows the K-value (in arbitrary units, A.U.) measured by the MetMet on large flat samples. The dashed line and the equation show the regression line. A value $\alpha = 3.58 \times 10^{-3}$ m^3 kg^{-1} that is the reciprocal of the slope is obtained. (b) Calibration of the size factor β. Ratio between the measurements with MetMet and KLY2 versus sample weight. Ideally, an infinite sample should give a ratio of 1, which is the asymptote of the fitting curve.

We computed a best-fitting curve, $\beta(m) = \frac{2}{\pi}\arctan\left(\frac{m}{62.5}\right)$, where the mass m is in g. This function designed to be β(m) = 1 in the large sample masses. This fitting curve accounts for most of the observed distribution down to a mass of 5 g (Figure 2b). Although the basalt samples that we used were rounded, some had shape anisotropy (i.e., flat or conical shape) that make them plot away from the trend curve (Table S3 and Figure S1). These samples were excluded from the computation of β(m). This indicates that measurements with the MetMet, as with other contact susceptibility probes like SM30, are sensitive to sample shape. Samples with strong shape anisotropy may provide less accurate results (see discussion in Gattacceca et al., 2004). Note that the calibration factor β was obtained for rocks with a density of 2900 kg m^{-3}. This is close to the usual range for most meteorites (e.g., Britt & Consolmagno, 2003). It is noteworthy that the departures from this a priori density (usually by a few tens of percent at most) result in changes in mass normalized magnetic susceptibility that are negligible compared to the three orders of magnitude covered by meteorite magnetic susceptibility. Finally, by combining Equations (1) and (4), the instrument can provide, once the sample mass is indicated using the rotative knob, the mass-normalized χ_m in logarithmic scale,

$$\log\chi_m = \log_{10}\left(\chi_m(m) \times 10^9\right) \quad (5)$$

which is displayed as "logχ value" on the instrument screen.

The second important function of this instrument is the estimation of the electrical conductivity of the sample. The impedance of the pick-up coil is a vector value and has sensitivities to the magnetic susceptibility and the conductivity of the sample (Dodd & Deeds, 1968). Kodama (2010) used a Lock-in amplifier to separate the in-phase (susceptibility) and the out-of-phase (conductivity or imaginary susceptibility) component between the excitation coil and the pick-up coil (i.e., mutual inductance). The MetMet has only a single coil and it cannot measure such out-of-phase component. Thus, the estimation of the conductivity is achieved by measuring the absolute value of the impedance of the LC resonator. The impedance of an ideal resonator without loss in oscillation is infinite. In reality, the coil and the capacitor consume energy due to the resistance of the coil and leakage current of the capacitor. Moreover, the presence of the sample induces additional losses (a phenomenon known as "iron-loss"). The impedance of the resonator (Z) decreases with increasing losses. In this instrument, we can safely assume that the resistance of the coil and the leakage current of the capacitor are constants. Therefore, the change in Z in comparison with the no-sample condition is entirely attributable to the presence of the sample and the associated iron losses. Indeed, in the presence of an electrically conductive sample, eddy currents are induced in the sample by the magnetic field applied from the oscillator (Faraday Law). Since such eddy currents are stronger at higher frequency, in order to enhance this effect, the MetMet operates at higher frequencies (100 kHz) than the other similar susceptibility meters (on

the order of 10 kHz or less). Finally, the energy of the resonator is consumed by Joule heating of the sample by the Eddy currents. The MetMet measures the absolute value of the impedance $|Z|$ as the amplitude of the oscillation. However, because the coil impedance change due to the eddy currents is a nonlinear process that also depends on the magnetic susceptibility (Bowler & Huang, 2005; Dodd & Deeds, 1968), it is difficult to derive the exact resistivity of the sample from this impedance measurement. Therefore, the MetMet provides a rough estimate of the conductivity, called "*C*-index," in arbitrary unit, computed with $|Z|$ and the magnetic susceptibility (see Appendix A). This *C*-index is designed to be positive and to be positively correlated with the electrical conductivity of the sample. Note that even for nonconductive rocks, some losses occur because of magnetic hysteresis in the sample, or other complex electromagnetic phenomena that are beyond the scope of this paper. This results in a non-zero *C*-index even for rocks that contain no metallic minerals. This must be considered for the interpretation of the *C*-index.

Massive metallic samples (e.g., iron meteorite, artificial steel, or aluminum objects) are the extreme conditions for MetMet operation as they stop the oscillation due to the excessive eddy current loss. In such case, the instrument detects the halt of the oscillation and indicates that the sample is metallic ("metal" displayed on the screen). Conversely, when there is no variation between f_{air} and f_{sample} ($K = 0$), the instrument indicates "low susceptibility" and gives a result for the theoretical detection limit of $\log\chi_m = 1$ (see Quality Control and the Detection Limit of the Instrument Section).

The instrument operation is simple. (1) The user pushes the knob (component 2 of Figure 1a) to start the "air" measurement and wait for 5 s. The MetMet must be kept at a distance of at least 10 cm from magnetic objects and metallic accessories (jewelry, metal fittings, etc.) during this measurement. The instrument measures f_{air} of Equation (2a). (2) The user places the sample at contact with the bottom of the instrument, pushes the knob again, and wait for 5 s. The instrument measures f_{sample} of Equation (2b). Subsequently, the instrument calculates the *K*-value of Equation (3) and indicates the $\log\chi$ value and *C*-index in logarithmic scale for the sample with infinite mass using Equations (4) and (5). (3) The user rotates the knob to input the sample mass. The instrument calculates $\beta(m)$ and indicates the mass-normalized $\log\chi_m$ value and *C*-index. The whole operation takes about 30 s.

Quality Control and the Detection Limit of the Instrument

The advantage of this instrument is that it does not require calibration of individual units. Indeed, since the *K*-value uses normalization by air measurement (Equation 3), the output of the MetMet is not sensitive to the exact properties of the electronic components. We used commercially available components with good tolerances (*R* and *C* in Figure 1b) and controlled that the inductance *L* of the custom-made coils is within 1% of the targeted value. The reproducibility of the measurements between units is guaranteed by the test using standard samples; but we do not need to calibrate the individual units.

All of the units that were produced over the last 5 years were tested by repeated measurements of identical samples (Figure 3). Sample description and raw data are available in Table S4 and Figure S2. This allows controlling the reproducibility of the results. The observed variations in *C*-index (standard deviations from 0.05 to 0.1 depending on rock types) and $\log\chi_m$ (SD from 0.03 to 0.06 depending on rock types) are not significant for the purpose of this instrument, since variations of 0.1–0.2 in $\log\chi_m$ or *C*-index do not influence identification and/or classification of meteorites whose intra-group variability is higher than that (Table 1, Figure 5).

The variation of $\log\chi_m$ in background measurements (Figure 3) is due to the uncertainty of the frequency counter and the instability of the *LC* oscillator (Figure 1b). According to the equations and the calibration factor α, $\log\chi_m = 1.25$ is approximately the theoretical detection limit of the MetMet whose frequency counter has the resolution of 2.5 ppm at the operating frequency (100 kHz). For this reason, the indication of $\log\chi_m$ is arbitrarily set to 1 for calculated values below 1. Equation (2b) assumes that the change in frequency is due only to the change in inductance caused by susceptibility of the sample. However, in reality, the capacitance can change by the temperature drift. The temperature coefficient of the capacitor used in the *LC* oscillator is ± 30 ppm $°C^{-1}$ at room temperature. Additionally, we use a crystal oscillator with stability of ± 20 ppm for the reference clock of the frequency counter. Assuming a maximum temperature drift of the electronics of 0.2°C during the 10 s long measurement procedure, the maximum total drift of the frequency is on the order of 10^{-5}, giving a background $\log\chi_m = 1.86$ in the worst case (Equations 3 and 4). This temperature-related drift in frequency is, unfortunately, not negligible due to the handling of this instrument. In practical terms, the detection limit of the MetMet is $\log\chi_m = 2$ as observed in Figure 3 (see Material Section S3 for the supplemental discussions). This error in the background drift is usually negligible for the most meteorites because the variation in frequencies due to the susceptibility of meteorites (the signal) is usually 10^{-4} or larger ($\log\chi_m > 2.5$). In this range, indeed, the uncertainty of $\log\chi_m$ is less than 0.1 as we demonstrated. Because *C*-Index has a dependency on $\log\chi_m$ (Appendix A), samples with low magnetic

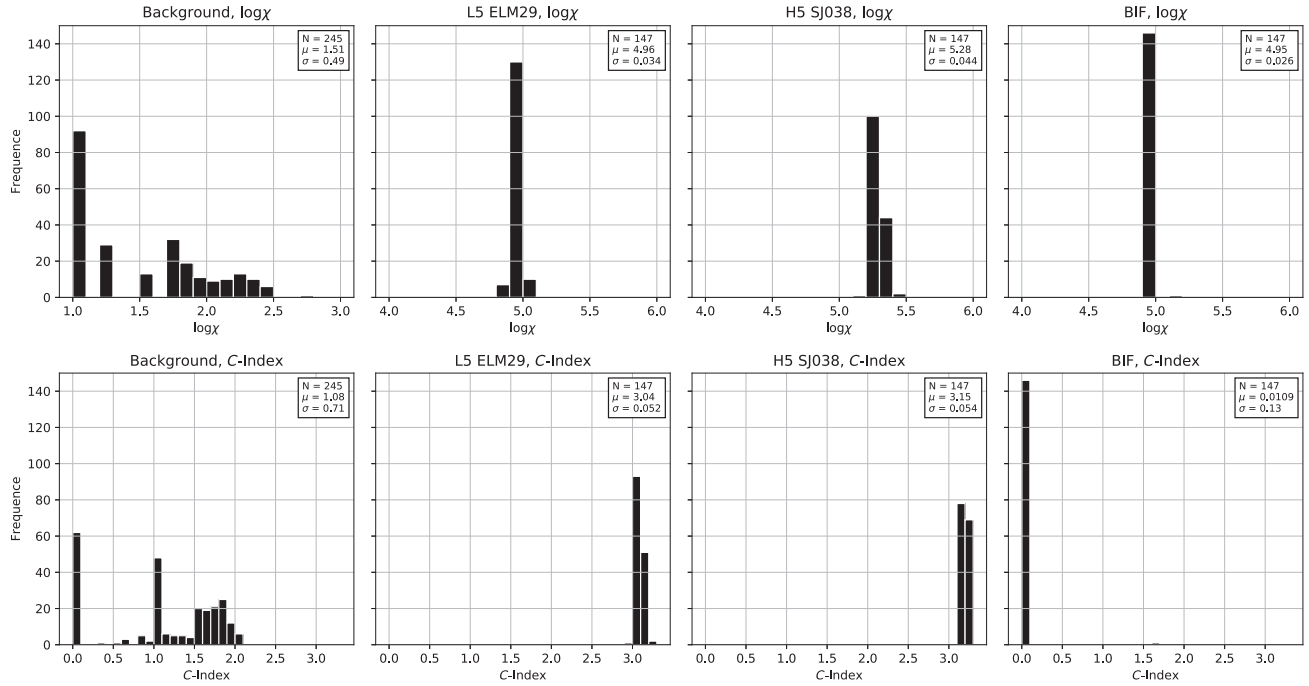

FIGURE 3. Histograms of measurements of the same samples using 49 different MetMet units. The size of bins is 0.1. The repetition times of measurements are at least three (for rocks and meteorites) and five measurements (for background measurements, with no sample present) for each unit. The number of measurements (N), the mean (μ), and the standard deviation (σ) are given in the inset box.

susceptibility will also have larger variability in C-index due to the relatively large drift in $\log\chi_m$. Although there are uncertainties for small samples with low $\log\chi_m$ samples, the MetMet has sufficient precision and accuracy to distinguish the different groups of meteorites.

It is noteworthy that although the MetMet operates at a different field amplitude and frequency compared to the KLY-2 and SM30 instruments that have been widely used to assemble meteorite susceptibility reference databases, no significant frequency dependence has been detected in most meteorites where it was tested (e.g., Gattacceca et al., 2014 for ordinary chondrites, and our own unpublished data). Similarly, no significant field dependence has been detected (our unpublished data) nor is it expected. Therefore, the susceptibility measurements performed with the MetMet can be safely compared to the published susceptibility values that have been measured with other instruments (e.g., Rochette et al., 2003, 2008, 2009).

MEASUREMENT OF METEORITES AND TERRESTRIAL ROCKS

Samples and Methods

We measured a total of 162 meteorite samples belonging to 25 meteorite groups (the data available in Table S6). The average sample mass is 39 g, ensuring that the measurements are representative of the bulk meteorite. This allowed exploring the $\log\chi_m$ versus C-index space covered by different groups. In a second step, we targeted specifically weathered ordinary chondrites (n = 143, average mass 97 g; Table S7), to study the effect terrestrial weathering on both parameters. All measured samples are from the CEREGE meteorite collection. Finally, 54 terrestrial rocks and minerals were measured for comparison with meteorites (Table S8).

The statistics are calculated by a Python script using Numpy, Scipy, Matplotlib, and Pandas modules (the script and the raw data are available in Material S2). The distribution of the $\log\chi_m$ and C-index is analyzed by a principal component analyses (PCA). The covariance matrix, the eigenvalue and the eigenvector of the covariance matrix are calculated to plot the confidence ellipse based on the chi-squared distribution. The confidence interval is 86%; this interval covers about two standard deviation (2σ) from the mean value. In Figure 4, we plot the confidence ellipse when the number of the sample is sufficient ($N \geq 3$) and the diameter of the confidence ellipse is not zero. Although the eigenvector and the eigenvalue are the essential metrics in the PCA, we provided here the semidiameters of the confidence ellipse and the slope of the principal

TABLE 1. Logχ_m and *C*-index of meteorite groups.

			Mean		SD		PCA			
Category	Group	*N*	*C*-index	Logχ_m	*C*-Index	Logχ_m	*a*	*b*	Slope	EVR PC_1
Magnetite dominated	All	29	2.01	4.40	0.23	0.59	1.21	0.25	3.00	0.96
	CK	9	2.16	4.84	0.07	0.13	0.26	0.14	6.22	0.78
	CV	16	1.93	4.12	0.22	0.62	1.27	0.23	3.40	0.97
	CVox	2	2.20	4.88	0.28	0.06	—	—	—	—
	CM	2	1.85	4.16	0.49	0.41	—	—	—	—
Pyrrhotite dominated	All	14	1.87	3.62	0.21	0.19	0.84	0.75	0.10	0.55
	Shergottite	5	1.96	3.69	0.11	0.28	0.56	0.22	−8.31	0.87
	R	9	1.82	3.59	0.24	0.13	0.48	0.25	−0.01	0.79
Metal dominated	All[a]	108	2.19	4.25	0.68	0.85	2.07	0.56	1.31	0.93
	EL	3	3.47	5.55	0.74	0.24	1.48	0.35	0.22	0.95
	H	7	3.11	5.36	0.17	0.15	0.36	0.27	0.69	0.65
	H/L	1	2.70	5.23	—	—	—	—	—	—
	L	9	2.74	4.92	0.15	0.11	0.36	0.09	0.68	0.94
	LL	7	1.77	3.87	0.20	0.25	0.56	0.26	1.41	0.83
	CH	1	2.90	5.40	—	—	—	—	—	—
	CO	11	2.08	4.52	0.20	0.36	0.74	0.34	2.98	0.82
	CR	2	2.60	5.17	0.00	0.02	—	—	—	—
	CVred	4	2.00	4.42	0.26	0.30	0.77	0.12	1.16	0.98
	Iron meteorites	6	4.58	5.13	0.53	0.31	1.14	0.38	−0.48	0.90
	Pallasite	5	4.22	5.61	0.52	0.12	1.02	0.22	0.09	0.96
	Mesosiderite	7	3.34	5.37	0.61	0.33	1.33	0.32	0.49	0.95
	Winonaite	1	4.00	5.55	—	—	—	—	—	—
	Acapulcoite	4	2.68	5.19	0.30	0.31	1.56	0.64	1.04	0.85
	Lodranite	1	2.30	4.72	—	—	—	—	—	—
	AcaLod	5	2.60	5.10	0.31	0.34	0.86	0.28	1.13	0.90
	Brachinite	2	1.85	3.94	0.07	0.59	—	—	—	—
	Ureilite	4	2.03	4.54	0.17	0.35	1.52	0.07	2.04	1.00
	BraUre	6	1.97	4.34	0.16	0.49	1.00	0.13	3.25	0.98
	Howardite	3	1.77	3.86	0.21	0.34	1.55	0.25	1.69	0.97
	Eucrite	23	1.71	3.29	0.27	0.37	1.49	0.98	2.59	0.70
	Eucrite (metal-rich)	2	1.70	4.23	0.42	0.24	—	—	—	—
	Diogenite	11	1.61	3.45	0.23	0.28	1.13	0.87	−2.72	0.63
	HED	37	1.69	3.38	0.25	0.37	0.73	0.48	4.32	0.70
	Lunar (feldsp. breccia)	5	1.60	3.48	0.20	0.25	0.52	0.36	2.26	0.67

Note: The number of the samples *N*, mean values and standard deviations of *C*-index and logχ_m, the semidiameters of the confidence ellipse (*a*, *b*), the slope of the first principal component are shown.
Abbreviations: AcaLod, acapulcoite + lodranite; BraUre, brachinite + ureilite; EVR PC_1, explained variance ratio of PC_1; HED, howardite + eucrite + diogenite; PCA, principal component analysis.
[a]Excluding iron meteorites and pallasites.

component axis. The complete statistical results are given in Table S5.

Results on Meteorites

A total of 25 meteorites groups were studied, with the rarest group represented by only a few meteorites. Within a meteorite group, logχ_m and *C*-index values are relatively well clustered (Figure 4). The PCA results (Table 1) show that for all meteorites groups, over 80% of the distribution can be explained by the first principal component (PC_1), that is, 80% of the total variance (explained variance ratio) is accounted for by the variance along PC_1 axes. This means that we can characterize the meteorite groups using their distribution in the logχ_m versus *C*-index space, in addition to the characterization using logχ_m only (e.g., Rochette et al., 2003, 2008, 2009).

As expected from previous comprehensive studies of the magnetic susceptibility of meteorites (e.g., Rochette et al., 2003, 2008, 2009), there is some overlap between some groups and variability within the groups. However, some groups can be separated. This is particularly true for the three groups of ordinary chondrites (Figure 4a)

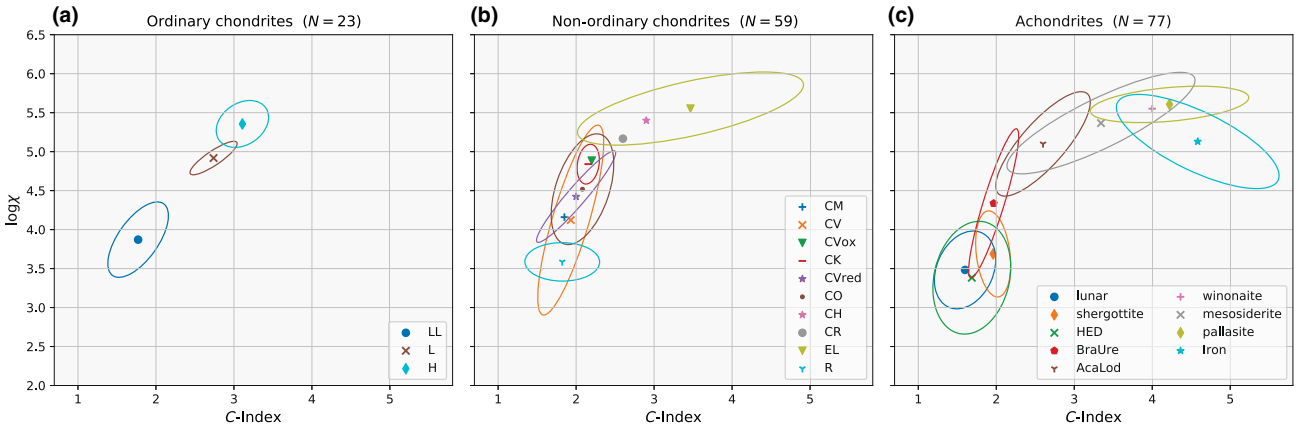

FIGURE 4. Distributions of $\log\chi_m$ and *C*-index for meteorite groups, represented by their 86% confidence ellipse and mean value. (a) Ordinary chondrites, (b) other chondrites, (c) achondrites and primitive achondrites excluding two anomalous metal-rich eucrites. Only the mean value is shown for groups represented by one or two meteorites.

that show an increase of the mean $\log\chi$ and *C*-index from LL to L and to H. The trend in $\log\chi_m$ has been already described in previous studies (Rochette et al., 2003) and is explained by the trend in the abundance of FeNi minerals. The trend in *C*-index has obviously the same origin.

The non-ordinary chondrite groups show strong overlaps as already observed by Rochette et al. (2008). Some groups show a widespread distribution, such as CV chondrites that cover the entire distribution of carbonaceous chondrites (Figure 4b). This is due to the variability of the magnetic mineralogy and associated magnetic properties of CVoxA, CVoxB, and CVred chondrites (Gattacceca et al., 2020). Other groups like CK chondrites have a more clustered distribution. The metal-rich non-ordinary chondrites (CH and CR) have high $\log\chi_m$ and *C*-index comparable to H and L chondrites.

Iron, stony-iron meteorites, EL chondrites, winonaites, and acapulcoites/lodranites have very high magnetic susceptibility ($\log\chi_m$ between 5.5 and 6.0) with saturation the instrument for the iron meteorites, but a steady increase of *C*-index.

When separating the meteorites according to their main magnetic minerals regardless of their classification, a clear distinction can be made between metal-dominated meteorites and magnetite-dominated meteorites (Figure 5). Pyrrhotite-dominated meteorites like Rumuruti chondrites ($N = 5$; Cournède et al., 2020) and shergottites ($N = 9$; Rochette et al., 2005) are not represented in these graphs because of the small number of measurements and meteorite groups involved. The slopes of the PC_1 of the magnetite- and metal-dominated meteorites are 3.0 and 1.3, respectively (Table 1). This indicates that the slope of the distribution is controlled by the ferromagnetic mineralogy, where the abundance of these minerals defines the position of the meteorites in this distribution. However, when a single meteorite is measured, it may be difficult to assign it to the metal- or magnetite-dominated group if the measurements plot near the intersection of the two distributions.

Effect of Terrestrial Weathering

Terrestrial weathering of metal-bearing meteorites leads to decrease of their magnetic susceptibility (see section Overlapping Susceptibility Ranges and Terrestrial Weathering). It must be noted, however, that when the weathering product is magnetite or maghemite, the magnetic susceptibility will not be affected because these two minerals have essentially the same magnetic susceptibility as metal. The electrical conductivity will always decrease with increasing weathering because of metal has a much higher conductivity than all iron oxides and oxyhydroxides.

To evaluate the effect of terrestrial weathering on the measurements performed with the MetMet, we measured 166 ordinary chondrites from the H, L, and LL groups, spanning weathering grades from W0 to W5 (Table 2). For L and H chondrites, a clear decrease of both magnetic susceptibility and *C*-index is observed with increasing weathering (Table 2, Figure 6a,b). For LL chondrites (Figure 6c), there is no clear trend with weathering, mostly because the fresh LL chondrites already span a rather wide magnetic susceptibility range, with in particular a decrease of $\log\chi_m$ with increasing petrographic type (Rochette et al., 2003). This pre-weathering variability of magnetic susceptibility in LL chondrites makes the effect of terrestrial weathering difficult to isolate.

Magnetic susceptibility and conductivity must be interpreted in the light of the weathering grade to provide

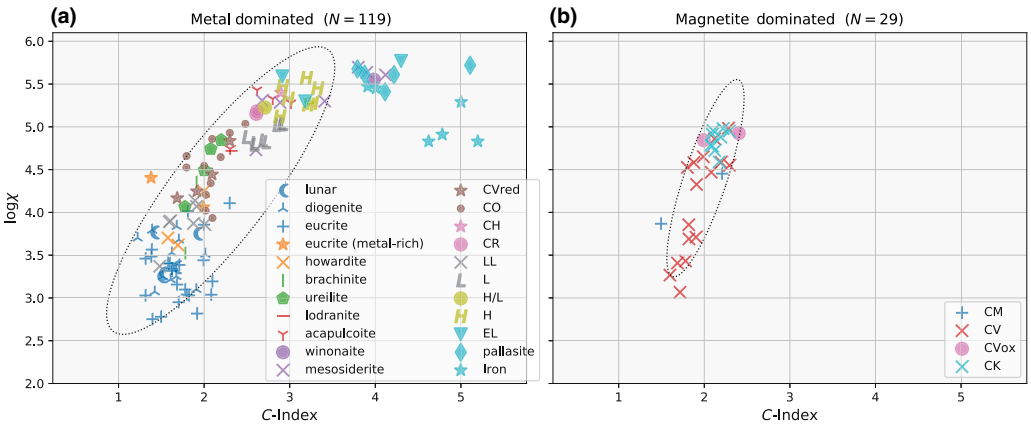

FIGURE 5. Logχ_m and *C*-index for meteorites, together with their 86% confidence ellipse. (a) Metal-dominated meteorites. (b) Magnetite-dominated meteorites. For metal-dominated meteorites, the overall confidence ellipse does not include iron meteorites and pallasite because of the saturation of the instrument.

TABLE 2. Logχ and *C*-index of weathered ordinary chondrites.

		Mean		SD		PCA			
Group/category	*N*	*C*-index	Logχ_m	*C*-index	Logχ_m	*a*	*b*	Slope	EVR PC_1
H (all W)	81	2.70	5.12	0.40	0.22	1.69	0.63	0.42	0.88
L (all W)	61	2.51	4.72	0.37	0.23	1.61	0.63	0.50	0.87
LL (all W)	24	1.80	3.99	0.33	0.29	1.36	1.04	0.60	0.63
H, W0	3	3.13	5.52	0.21	0.05	0.83	0.13	0.17	0.98
H, W1	20	3.01	5.29	0.29	0.13	1.17	0.43	0.24	0.88
H, W2	30	2.76	5.14	0.35	0.16	1.40	0.59	0.15	0.85
H, W3	21	2.43	4.96	0.29	0.16	1.13	0.63	0.10	0.76
H, W4	6	2.17	4.75	0.18	0.08	0.70	0.31	0.20	0.84
L, W0	2	2.68	4.90	0.04	0.11	—	—	—	—
L, W1	16	2.69	4.87	0.24	0.12	1.01	0.35	0.38	0.89
L, W2	11	2.47	4.63	0.49	0.29	2.10	0.74	0.48	0.89
L, W3	21	2.39	4.64	0.41	0.19	1.66	0.65	0.27	0.87
L, W4	3	2.17	4.40	0.12	0.23	0.93	0.37	−3.03	0.86
L, W5	1	2.30	4.64	—	—	—	—	—	—
LL, W0	1	1.90	4.14	—	—	—	—	—	—
LL, W1	11	1.78	4.00	0.32	0.22	1.32	0.78	0.36	0.74
LL, W2	4	1.68	3.88	0.39	0.44	1.79	1.49	−2.06	0.59
LL, W3	4	1.92	4.14	0.39	0.25	1.70	0.70	0.49	0.86
LL, W4	4	2.05	4.01	0.17	0.48	1.97	0.42	3.44	0.96
LL, W5	1	1.30	3.88	—	—	—	—	—	—

Note: The number of the samples *N*, mean values and standard deviations of *C*-index and logχ_m, the semidiameters of the confidence ellipse (*a, b*), the slope of the first principal component are shown.
Abbreviations: EVR PC_1, explained variance ratio of PC_1; PCA, principal component analysis; W, weathering grade.

accurate classification of ordinary chondrites. In particular, intense weathering results in an overlap of the magnetic susceptibility and *C*-index of weathered H chondrites with L chondrites, and of weathered L chondrites with LL chondrites (Figure 6d). In that case, magnetic classification is not possible, and other methods must be used.

Terrestrial Rocks and Artificial Materials

Most of the terrestrial rocks and minerals have lower *C*-index values than most meteorites (Figure 7, Table S1). Many of them have very low (<1) or zero *C*-index. However, a number of rocks overlap with the meteorite in the logχ_m versus *C*-index space. Notably, a significant

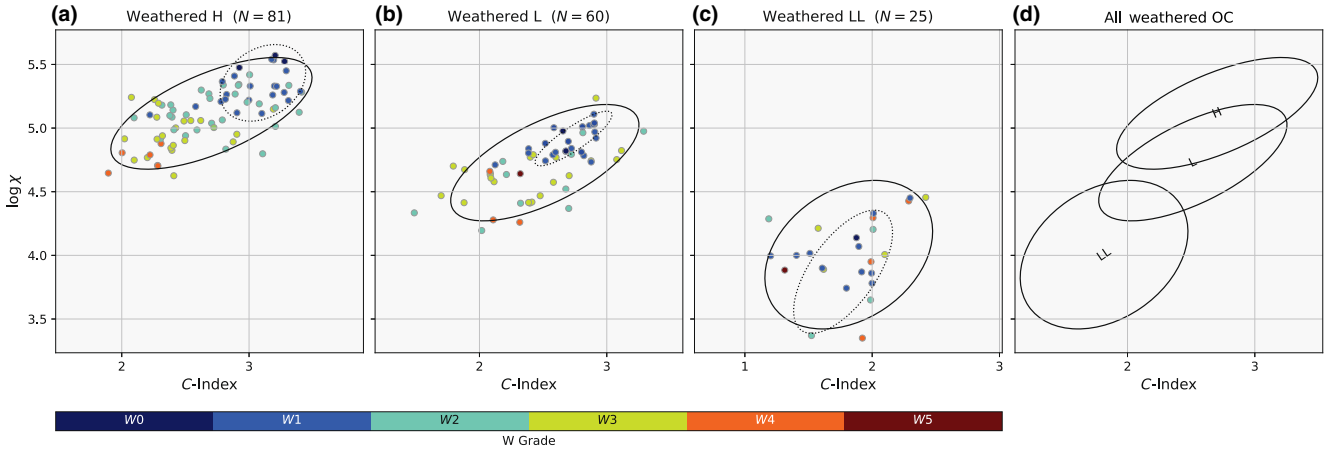

FIGURE 6. *C*-index and $\log\chi_m$ of ordinary chondrites as a function of their weathering grade (color coded). The solid (respectively, dashed) ellipses are the 86% confidence ellipses of the distribution for all meteorites (respectively unweathered meteorites). (a) H chondrites, (b) L chondrites, (c) LL chondrites, (d) all ordinary chondrites.

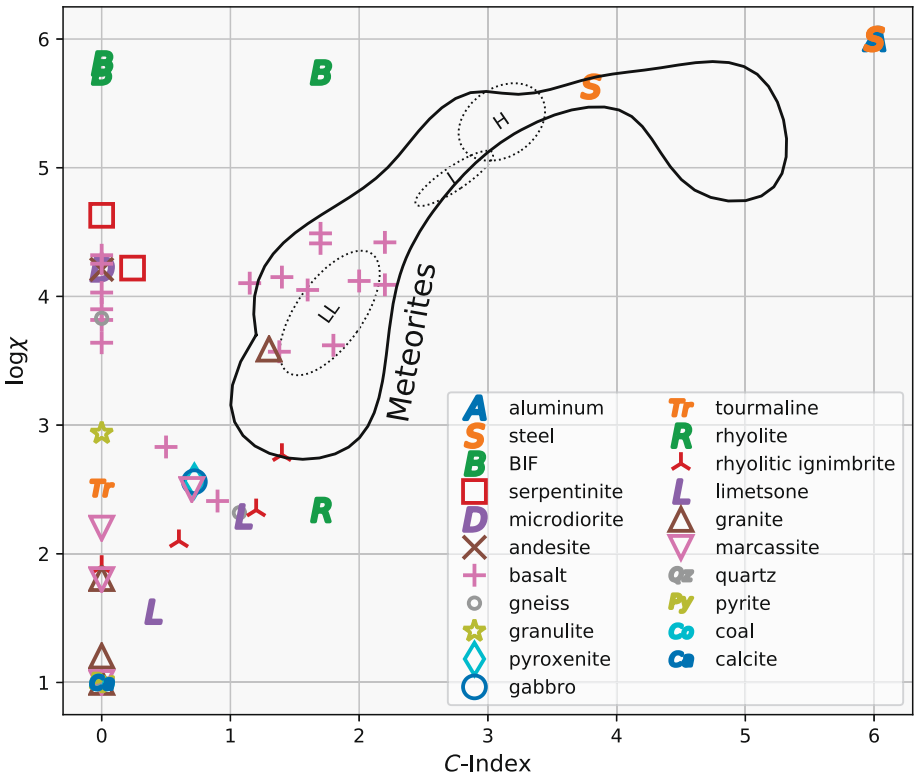

FIGURE 7. $\text{Log}\chi_m$ and *C*-index of a selection of terrestrial rocks and minerals, and artificial samples. Samples that have a signal below the detection limit (coal and calcite) are plotted at arbitrarily at $\log\chi_m = 1$ and *C*-index = 0. Samples that give "metal" indication are plotted arbitrarily at $\log\chi_m = 6$ and *C*-index = 6. The overall distribution of meteorites is shown by the solid line. The distribution for the three ordinary chondrite groups is shown by the dashed lines (86% confidence ellipses).

population of terrestrial basalts have almost same distribution of $\log\chi_m$ and *C*-index than the LL chondrites. Since they contain no metallic phases or other electrically conductive minerals (e.g., native copper or gold), this increase in *C*-index may result from the detection of the out-of-phase component of the susceptibility due to the presence of superparamagnetic grains (Kodama, 2013). Indeed, the MetMet uses high-frequency AC magnetic

fields of order of 100 kHz that can efficiently induce an out-of-phase component. This theoretical possibility would require experimental confirmation.

CONCLUSION

The MetMet instrument allows the measurement of magnetic susceptibility and a conductivity proxy (*C*-index) of rocks and artificial objects. The electrical consumption of the instrument is low, ensuring long battery life. The instrument is portable and easy to use with a single knob and a simple measurement protocol. Measurements are fast (30 s) and when provided with a rough sample mass estimate, the instrument displays the susceptibility result in mass-normalized units ($\log\chi_m$, with χ_m in 10^{-9} m^3 kg^{-1}), making the interpretation straightforward for users that have little knowledge of rock magnetism, and/or in the field. The instrument is precise and accurate enough to allow distinguishing most meteorites from most terrestrial rocks, and to provide guidance in the classification of meteorites. The recommended minimum sample mass is 5 g. The instrument has been used successfully by meteorites hunters, meteorite collectors, meteorite dealers, and for outreach activities, as non-specialists, including children, are able to operate it easily. The interpretation of the data can be limited to separating terrestrial rocks from meteorites, or can be performed at a higher level by separating different groups of meteorites. It is noteworthy that this kind of measurements is highly preferable to the use of hand magnets that has poor diagnostic value and permanently affects the paleomagnetic record of meteorites.

Acknowledgments—We thank the two reviewers, S. Tikoo and T. Kohout, and the Associate Editor, K. Joy, for their detailed and constructive reviews of this manuscript. This study was partially supported by the Agence Nationale de la Recherche (project FRIPON, number ANR13-BS05-0009) and the Vigie-Ciel outreach program. Mariko U. wound up all of the MetMet pick-up coils, measured the calibration basalt pebbles, and tested each unit after assembly.

Editorial Handling—Dr. Katherine Helen Joy

REFERENCES

Bowler, N., and Huang, Y. 2005. Electrical Conductivity Measurement of Metal Plates Using Broadband Eddy-Current and Four-Point Methods. *Measurement Science and Technology* 16: 2193–2200.

Britt, D. T., and Consolmagno, G. J. 2003. Stony Meteorite Porosities and Densities: A Review of the Data through 2001. *Meteoritics & Planetary Sciences* 38: 1161–80.

Colas, F., Zanda, B., Bouley, S., Jeanne, S., Malgoyre, A., Birlan, M., Blanpain, C., et al. 2020. FRIPON: A Worldwide Network to Track Incoming Meteoroids. *Astronomy & Astrophysics* 644: A53.

Consolmagno, G. J., Macke, R. J., Rochette, P., Britt, D. T., and Gattacceca, J. 2006. Density, Magnetic Susceptibility, and the Characterization of Ordinary Chondrite Falls and Showers. *Meteoritics & Planetary Sciences* 41: 331–342.

Cournède, C., Gattacceca, J., Rochette, P., and Shuster, D. L. 2020. Paleomagnetism of Rumuruti Chondrites Suggests a Partially Differentiated Parent Body. *Earth and Planetary Science Letters* 533: 116042. https://doi.org/10.1016/j.epsl.2019.116042.

Di Cecco, V. E., Hyde, B. C., Tait, K. T., and Nicklin, R. I. 2022. Determination of Olivine Fayalite-Forsterite Composition 1 in Ordinary Chondrites by X-Ray Diffraction. *Meteoritics & Planetary Science* 57: 1288–99. https://doi.org/10.1111/maps.13824.

Dodd, C., and Deeds, W. 1968. Analytical Solutions to Eddy-Current Probe-Coil Problems. *Journal of Applied Physics* 39: 2829–38.

Folco, L., Rochette, P., Gattacceca, J., and Perchiazzi, N. 2006. In Situ Identification, Pairing and Classification of Meteorites from Antarctica through Magnetic Susceptibility Measurements. *Meteoritics & Planetary Science* 41: 343–353.

Gattacceca, J., Bonal, L., Sonzogni, C., and Longerey, J. 2020. CV Chondrites: More than One Parent Body. *Earth and Planetary Science Letters* 147: 116467.

Gattacceca, J., Eisenlohr, P., and Rochette, P. 2004. Calibration of *In Situ* Magnetic Susceptibility Measurements. *Geophysical Journal International* 158: 42–49.

Gattacceca, J., Mccubbin, F., Grossman, J., Bouvier, A., Bullock, E., Chennaoui, A. H., Debaille, V., et al. 2021. The Meteoritical Bulletin, No. 109. *Meteoritics & Planetary Science* 56: 1626–30. https://doi.org/10.1111/maps.13714.

Gattacceca, J., and Rochette, P. 2004. Toward a Robust Normalized Magnetic Paleointensity Method Applied to Meteorites. *Earth and Planetary Science Letters* 227: 377–393.

Gattacceca, J., Suavet, C., Rochette, P., Weiss, B. P., Winklhofer, M., Uehara, M., and Friedrich, J. 2014. Metal Phases in Ordinary Chondrites: Magnetic Hysteresis Properties and Implications for Thermal History. *Meteoritics & Planetary Science* 49: 652–676.

Jarosewich, E. 1990. Chemical Analysis of Meteorites: Compilation of Stony and Iron Meteorite Analyses. *Meteoritics* 25: 323–337.

Kodama, K. 2010. A New System for Measuring Alternating Current Magnetic Susceptibility of Natural Materials over a Wide Range of Frequencies. *Geochemistry, Geophysics, Geosystems* 11: Q11002. https://doi.org/10.1029/2010GC003303.

Keil, K., and Frederiksson, K. 1964. The Iron, Magnesium and Calcium Distribution in Coexisting Olivines and Rhombic Pyroxenes of Chondrites. *Journal of Geophysical Research* 69: 3487–3515.

Kodama, K. 2013. Application of Broadband Alternating Current Magnetic Susceptibility to the Characterization of Magnetic Nanoparticles in Natural Materials. *Journal of Geophysical Research: Solid Earth* 118: 1–12. https://doi.org/10.1029/2012JB009502.

Lunning, N., Corrigan, C., Welzenbach, L., and McCoy, T. 2012. Using Immersion Oils to Classify Equilibrated Ordinary Chondrites from Antarctica. 43rd Lunar and Planetary Science Conference, abstract #1566, p. 1566.

Metzler, K. 2018. From 2D to 3D Chondrule Size Data: Some Empirical Ground Truths. *Meteoritics & Planetary Science* 53: 1489–99.

Munayco, P., Munayco, J., De Avillez, R. R., Valenzuela, M., Rochette, P., Gattacceca, J., and Scorzelli, R. B. 2013. Weathering of Ordinary Chondrites from the Atacama Desert, Chile, by Mössbauer Spectroscopy and Synchrotron Radiation X-Ray Diffraction. *Meteoritics & Planetary Science* 48: 457–473.

Rochette, P., Gattacceca, J., Bonal, L., Bourot-Denise, M., Chevrier, V., Clerc, J.-P., Consolmagno, G., et al. 2008. Magnetic Classification of Stony Meteorites: 2. Non-Ordinary Chondrites. *Meteoritics & Planetary Sciences* 43: 959–980.

Rochette, P., Gattacceca, J., Bourot-Denise, M., Consolmagno, G., Folco, L., Kohout, T., Pesonen, L., and Sagnotti, L. 2009. Magnetic Classification of Stony Meteorites: 3. Achondrites. *Meteoritics & Planetary Sciences* 44: 405–427.

Rochette, P., Gattacceca, J., Chevrier, V., and Lorand, J. P. 2005. Matching Martian Crustal Magnetization and Meteorite Magnetic Properties. *Meteoritics & Planetary Sciences* 40: 529–540.

Rochette, P., Gattacceca, J., and Lewandowski, M. 2012. Magnetic Classification of Meteorites and Application to the Soltmany Fall. *Meteorites* 2: 67–71. https://doi.org/10.5277/met120108.

Rochette, P., Sagnotti, L., Bourot-Denise, M., Consolmagno, G., Folco, L., Gattacceca, J., Osete, M. L., and Pesonen, L. 2003. Magnetic Classification of Stony Meteorites: 1 Ordinary Chondrites. *Meteoritics & Planetary Sciences* 38: 251–58.

Savitsky, Z. 2023. Magnets Wipe Memories from Meteorites. *Science* 380: 17–18. https://doi.org/10.1126/science.adi1219.

Uehara, M., Gattacceca, J., Rochette, P., Demory, F., and Valenzuela, E. M. 2012. Magnetic Study of Meteorites Recovered in the Atacama Desert (Chile): Implications for Meteorite Paleomagnetism and the Stability of Hot Desert Surfaces. *Physics of the Earth and Planetary Interiors* 200-201: 113–123.

Vervelidou, F., Weiss, B., and Lagroix, F. 2023. Hand Magnets and the Destruction of Ancient Meteorite Magnetism. *Journal of Geophysical Research-Planets*, forthcoming 128: e2022JE007464. https://doi.org/10.1029/2022JE007464.

Weiss, B. P., Gattacceca, J., Stanley, S., Rochette, P., and Christensen, U. R. 2010. Paleomagnetic Records of Meteorites and Early Planetesimal Differentiation. *Space Science Reviews* 152: 341–390. https://doi.org/10.1007/s11214-009-9580-z.

Wlotzka, F. 1993. A Weathering Scale for the Ordinary Chondrites. *Meteoritics* 28: 460.

Zurfluh, F. J., Hofmann, B. A., Gnos, E., and Eggenberger, U. 2011. Evaluation of the Utility of Handheld XRF in Meteoritics. *X-Ray Spectrometry* 40: 449–463. https://doi.org/10.1002/xrs.1369.

SUPPORTING INFORMATION

Additional supporting information may be found in the online version of this article.

Data S1.
Material S2.
Table S1.

APPENDIX A CALCULATION OF THE CONDUCTIVITY PROXY (*C*-INDEX)

The *C*-Index is the simple proxy of the conductivity of the sample for a magnetic susceptibility meter with a single coil that is based on the amplitude of the oscillation. As well as the magnetic susceptibility measurements, the instrument measures the amplitude of the oscillation with and without sample (V_{air} and V_{sample}, respectively). These voltages are the proxy of the absolute value of the impedance $|Z|$ of the resonator. To separate the contribution of the conductivity from the actual *C*-index in this article is calculated as following:

$$\begin{cases} C-\text{index} = \log_{10}(a \times C + b \times D) \\ C = \dfrac{V_{air}}{V_{sample}} - 1 \\ D = \dfrac{K'}{K'+1}, K' = \dfrac{K}{\beta(m)} \times e + f \end{cases},$$

where a, b, e, and f are constants (respectively, 21,650, 16,650, 0.9, and 0.1), K the value defined by Equation (3), and β the calibration factor used in Equation (4). The first term in the logarithm ($a \times C$) calculates the normalized impedance Z', and the second term ($b \times D$) compensates the effect of the magnetic susceptibility on the Z' changing. V_{sample} diminishes because of iron loss due to the sample conductivity. As a result, the C value and *C*-index increase with the conductivity of the sample. The constants are calibrated by measurements of the banded iron formation (BIF) samples that do not contain metal grains, being *C*-index = 0. This *C*-index is based on the circuit analysis and the empirical method but is not based on the analytical solutions of eddy current by Dodd and Deeds (1968) and Bowler and Huang (2005).